Supplemental information

“The Psychosis Human Connectome Project: Design and rationale for studies of visual neurophysiology”

Michael-Paul Schallmo, Kimberly B. Weldon, Rohit S. Kamath, Hannah R. Moser, Samantha A. Montoya, Kyle W. Killebrew, Caroline Demro, Andrea N. Grant, Małgorzata Marjańska, Scott R. Sponheim, Cheryl A. Olman

NeuroImage

Supplemental background

One of the most fundamental functions in the visual system is contrast perception, which is impaired in psychosis spectrum disorders including schizophrenia and bipolar disorder (Butler et al., 2007; Butler et al., 2005; Calderone et al., 2013; Fernandes et al., 2019; Keri et al., 2002; Lalor et al., 2012; Martinez et al., 2008; Skottun and Skoyles, 2007; Slaghuis and Bishop, 2001; Yoon et al., 2009). Visual contrast is the difference in luminance between adjacent pixels or image regions. Electrophysiological studies of early visual cortex in animal models show that neurons have nonlinear contrast-response functions (i.e., the relationship between input, or visual stimulus contrast, and output, or neural response), with response saturation occurring at high contrast (Albrecht and Hamilton, 1982; Sclar et al., 1990). This is often referred to as contrast gain control and is thought to reflect a balance between local excitatory and inhibitory processes (Butler et al., 2008; Carandini and Heeger, 2012; Katzner et al., 2011). Similar nonlinearities are observed in human contrast perception (Boynton et al., 1999; Legge and Foley, 1980; Yu et al., 2003). Studies in humans have used psychophysical and functional MRI methods to link performance in visual contrast perception tasks to the magnitude of neural responses in early visual areas such as primary visual cortex (V1; Boynton et al., 1999; Olman et al., 2004; Zenger-Landolt and Heeger, 2003). With regard to psychotic disorders, early work indicated that impaired contrast perception might reflect a specific magnocellular deficit (Butler et al., 2007; Butler et al., 2005; Keri et al., 2002; Martinez et al., 2008), whereas more recent studies have suggested that contrast perception may be impaired more generally (i.e., for both magnocellular and parvocellular pathways; Calderone et al., 2013; Lalor et al., 2012; Skottun and Skoyles, 2007). A few studies have applied neuroimaging tools to investigate impaired contrast perception in PwPP, with some evidence suggesting reduced neural responses in early visual cortex (Butler et al., 2007; Calderone et al., 2013; Lalor et al., 2012; Martinez et al., 2008).

Another visual function that appears disrupted among PwPP is visual context perception. Spatial context phenomena refer to the modulation (either enhancement or suppression) of the perception of a centralized visual target by surrounding stimuli. For example, surround suppression is a visual effect (illusion) in which the perceived salience of a center stimulus (e.g., the contrast of a sinusoidal grating) is reduced in the presence of a surrounding stimulus (e.g., a high contrast annular grating; Cai et al., 2008; Chubb et al., 1989; Petrov and McKee, 2006; Schallmo and Murray, 2016; Snowden and Hammett, 1998; Xing and Heeger, 2000, 2001; Yu et al., 2001; Yu et al., 2003). This perceptual suppression corresponds with suppressed neural activity (as measured by fMRI in humans) in early visual areas such as V1 (Chen, 2014; Joo et al., 2012; Nurminen et al., 2009; Pihlaja et al., 2008; Poltoratski et al., 2017; Schallmo et al., 2016; Self et al., 2016; Vanegas et al., 2015; Williams et al., 2003; Zenger-Landolt and Heeger, 2003), consistent with electrophysiological studies in animal models showing suppression of neural responses to stimuli inside the classical receptive field by surrounding stimuli (Angelucci and Bressloff, 2006; Bair et al., 2003; Cavanaugh et al., 2002; Shushruth et al., 2013; Walker et al., 1999; Webb et al., 2005). Studies of surround suppression in people with psychotic disorders have generally shown weaker suppression effects (i.e., reduced illusion strength, or more veridical perception), especially among people with schizophrenia (Barch et al., 2012; Dakin et al., 2005; Schallmo et al., 2015; Serrano-Pedraza et al., 2014; Tadin et al., 2006; Tibber et al., 2013; Yang et al., 2013b; Yoon et al., 2009), and

to perhaps a lesser extent among people with bipolar disorder (Schallmo et al., 2015; Yang et al., 2013a); for a meta-analysis, see (Linares et al., 2020). Relatively few studies have examined the physiological basis of reduced surround suppression in psychotic psychopathology; those few have suggested there might be impaired inhibition by GABA (Yoon et al., 2010) and / or reduced neural suppression (Anderson et al., 2017; Seymour et al., 2013) in early visual cortex.

Aspects of perceptual organization, including visual contour integration and perception of more complex forms / objects, also appear to be disrupted among PwPP. Contour perception involves detecting visual edges or boundaries, which is a critical step for distinguishing visual objects from background stimuli (i.e., figure-ground segmentation), and is important for navigating a visual environment (Loffler, 2008). Contour detection is often studied using tasks that require participants to integrate spatially separated elements; studies in healthy adults generally show that contour perception follows the Gestalt principles of proximity and good continuation (Loffler, 2008; Wertheimer, 1938). Perception of visual forms or objects involves the integration of one or more visual edges or contours, which facilitates perception of an isolated and / or closed visual shape. Processing of visual contours and shapes is reflected in neural responses in human V1 and in higher visual areas such as the lateral occipital complex (LOC) as measured by fMRI (Altmann et al., 2003; Keane et al., 2021; Murray et al., 2002; Qiu et al., 2016), in agreement with electrophysiological studies in animal models (Bauer and Heinze, 2002; Li et al., 2006; Li et al., 2008). Behavioral studies have repeatedly demonstrated impaired detection and discrimination of fragmented visual contours among people with schizophrenia (Grove et al., 2018; Keane et al., 2016; Pokorny et al., 2021b; Robol et al., 2013; Schallmo et al., 2013; Silverstein et al., 2006; Silverstein et al., 2012; Silverstein et al., 2000), as well as impaired perception of illusory contours (e.g., Kanizsa figures; Keane et al., 2014; Keane et al., 2018). A few fMRI studies have linked impaired contour integration in schizophrenia to abnormal neural processing in mid-level visual areas such as LOC (Silverstein et al., 2009; Silverstein et al., 2015). There is also evidence for impaired perception of more complex visual objects or forms among PwPP, including fragmented objects (Pokorny et al., 2021a), Mooney faces (Rivolta et al., 2014; Uhlhaas et al., 2006), and global motion percepts (Bennett et al., 2016; Carter et al., 2017; Chen et al., 2005). However, our understanding of the neural basis of impaired perceptual organization among PwPP remains somewhat limited.

It has been proposed that abnormal visual perception among PwPP may depend on an imbalance between excitation / inhibition (E/I) in brain regions related to visual perception (Foss-Feig et al., 2017; Lisman, 2012). E/I functions have been investigated behaviorally among healthy adults using bi-stable visual paradigms, such as binocular rivalry or the rotating cylinder illusion (Mentch et al., 2019; Robertson et al., 2016; van Loon et al., 2013). Bi-stable paradigms involve presenting a single visual stimulus with two competing perceptual interpretations, with the participant's perceptual experience spontaneously alternating between the two. Previous work has suggested that differences across individuals or groups in the rate of alternation of bi-stable percepts may be related to differences in E/I functioning (Mentch et al., 2019; Robertson et al., 2016; van Loon et al., 2013). Abnormal bi-stable perception has been reported among PwPP as compared with controls (Fox, 1965; Miller et al., 2003; Nagamine et al., 2009; Ngo et al., 2011; Schmack et al., 2017; Schmack et al., 2015; Xiao et al., 2018; Ye et al., 2019), which may be consistent with an E/I imbalance in visual cortex.

There are several major challenges associated with acquiring fMRI and / or MRS data at 7 tesla (Godlewska et al., 2017; Henning, 2018; Olman and Yacoub, 2011), in addition to the advantages noted in the Introduction. These include: 1) inhomogeneity of the static magnetic field (B_0), 2) inhomogeneous transmit and receive B_1, 3) limited radiofrequency amplifier power, and 4) shorter T_2 relaxation times. Static B_0 inhomogeneities (e.g., at the interface of different tissue types) result in geometric distortions that scale linearly with increasing B_0 field strength (Dymerska et al., 2018). This makes effective approaches for mitigating geometric distortion, such as prospective B_0 shimming and retrospective distortion compensation methods, especially important for studies at 7 T (Schallmo et al., 2021). In the current study, we performed prospective B_0 shimming prior to MRS and fMRI data collection, and acquired a single gradient echo EPI scan with an opposite phase encoding (PE)

direction, to facilitate retrospective geometric distortion compensation of our fMRI data. In addition, the wavelength of the radiofrequency pulse at 7 T is on the order of 12 cm (Godlewska et al., 2017; Van de Moortele et al., 2005), which is shorter than at lower field strengths, and is approximately equal to the average size of a human head. This results in patterns of destructive interference across the brain, which we refer to as transmit B_1 inhomogeneity. There are a number of approaches that seek to address transmit B_1 efficiency and inhomogeneity, which include the use of dielectric pads (Vu et al., 2015) to improve transmit efficiency, and B_1 shimming to improve efficiency and homogeneity on parallel transmit systems using either static (Emir et al., 2012; Van de Moortele et al., 2005) or dynamic (Wu et al., 2013) techniques. The present study used coils (NOVA32 and quadrature surface coils) which do not have parallel transmit capabilities. To improve transmit B_1 efficiency during fMRI studies, dielectric pads were used. Finally, shorter T_2 relaxation times at 7 T (compared to lower field strengths) make it advantageous to use shorter TE and / or echo spacing (Godlewska et al., 2017; Olman and Yacoub, 2011), but this may impose some additional hardware constraints (e.g., sufficiently fast gradient slew rates, parallel imaging capabilities). For the current study, we chose an ultra-short TE (8 ms) STEAM sequence for MRS, and our GE EPI sequence for fMRI (TE = 22.2 ms, echo spacing = 0.64 ms, parallel imaging acceleration factor = 2) followed the 7 T fMRI protocol in the original Young Adult HCP (Glasser et al., 2016; Van Essen et al., 2013; Vu et al., 2017; Vu et al., 2015).

Supplemental methods

Clinical measures

We collected questionnaire and interview-based measures related to clinical psychiatric status outside of the scanner, prior to the MR experiments. These included the Brief Psychiatric Rating Scale (BPRS, 24 item version; Ventura et al., 2000), the Scale for the Assessment of Negative Symptoms (SANS; Andreasen, 1982), the Scale for the Assessment of Positive Symptoms (SAPS; Andreasen, 1984), the Positive and Negative Affect Schedule (PANAS; Watson et al., 1988), and a questionnaire about sleep habits and recent use of prescription and non-prescription drugs. BPRS, PANAS, and the sleep and recent use questionnaire were collected for all individuals, while SAPS and SANS were collected only for PwPP. Because the BPRS, SAPS, and SANS reflect clinical symptom levels over the past month, these measures were collected on the day of 7 T scanning, unless the participant had completed them during another research visit within 30 days of the 7 T scan. These measures were collected at each visit for participants who completed two scanning sessions (e.g., 7T-B and 7T-Z). We observed a modest degree of variability in BPRS, SAPS, and SANS scores among PwPP between the first and second scanning sessions (Supplemental Table 3 and Supplemental Figure 2) indicating that symptoms levels varied to some extent over time within this group, as expected (Long and Brekke, 1999).

Other clinical data used in this study were collected on a separate clinical research visit on a different day, prior to the 7 T session. These included the Sensory Gating Inventory (SGI; Hetrick et al., 2012), the Schizotypal Personality Questionnaire (SPQ; Raine, 1991), and the Personality Inventory for DSM-5 (PID-5; Krueger et al., 2012), which includes a psychoticism factor score. Full details of our clinical measures are reported in our companion paper (Demro et al., 2021). Table 1 shows a summary of the data from different clinical measures for each group.

Prior to completing visual psychophysics and 7 T MR experiments, the participant's visual acuity was assessed using a Snellen eye chart (Snellen, 1862) from a viewing distance of 100 cm and a height of 140 cm from the floor. Acuity data are presented in Table 1. Participants wore corrective lenses as needed; MR compatible frames and lenses were provided, and were worn during all experiments on the 7 T scanning day. The experimental protocol was discontinued for participants who did not demonstrate visual acuity (including correction) of 20/40 (decimal fraction = 0.5) or better. Other visual measures were collected from all participants during an earlier, clinically focused study visit. These include: visual questionnaires from the NIH PhenX Toolkit (i.e., Contact Lens Use, Personal and Family History of Eye Disease and Treatments, Personal and Family History of Strabismus, Visual Function questions about eyesight and driving), Mars Letter Contrast

Sensitivity test (Arditi, 2005), and the Farnsworth Dichotomous Color Vision test (Farnsworth, 1943), as described in our companion paper (Demro et al., 2021).

Protocol nomenclature

Our first iteration of the protocol was termed version 'A.' 7T-A scans began in July 2017 and did not include MRS data from prefrontal cortex, as the radiofrequency (RF) head coil used for these scans was not yet available. Other data are also missing from some early 7T-A scans due to technical issues (for information about the number of datasets available from each protocol version, see Supplemental Table 2). In January 2018, we began collecting data from the second iteration of our experimental protocol, which we refer to as 7T-B. Here, we added MRS data collection from a region of the dorsomedial prefrontal cortex, as described in the MR spectroscopy section of the Methods. We also made some small changes to the visual stimuli and paradigms in the CSS (psychophysics) and COP (psychophysics and fMRI) tasks (see below). We refer to repeat scans in which the 7T-B protocol was repeated as 7T-Z. In some cases, participants completed both 7T-A and 7T-B protocols; for these, the second scan is referred to as 7T-B. In other cases, individuals participated in both 7T-B and 7T-Z scans, but did not complete the full scanning protocol during 7T-B. In these cases, the scan data from the second visit are still labeled as 7T-Z, even though the 7T-B imaging data are incomplete or missing.

Task versions

Between July and December 2017, an initial group of 27 participants (20 controls, 7 PwPP) completed our initial experimental protocol, which we refer to as 7T-A. Following examination of the data from this initial pilot phase, modifications were made to the CSS (psychophysics) and COP (psychophysics and fMRI) paradigms, which are detailed below. The number of data sets collected from each version of these tasks is described in Supplemental Table 2.

For the CSS experiment, as part of the transition to 7T-B we added a 0.65% contrast pedestal condition (with no surround) to the psychophysical task to better capture the expected 'dipper' phenomenon in the threshold versus contrast data (i.e., thresholds at very low pedestal contrasts that are lower than the detection threshold; see Figure 8B). We also increased the maximum value of the contrast increment from 20% to 40%, in order to better address cases in which participants struggled to discriminate stimuli with relatively large contrast increments. As the contrast increment during catch trials was fixed at the maximum value, this change also increased the increment on catch trials from 20% to 40%.

For the COP experiment, we reduced the background clutter as part of the change to the 7T-B protocol, in order to make the task easier. To this end, we decreased the number of background Gabor elements (from 207 to 155) and increased their minimum spacing (from 0.7° to 0.8°). This had the effect of increasing the SNR for the contour stimuli (i.e., background versus contour element spacing) from 0.75 to 0.87.

Data processing

For both fMRI and MRS, T_1-weighted structural MRI data acquired in a separate scanning session at 3T were used as an anatomical reference scan (i.e., for co-registration, below). Anatomical data (T_1- and T_2-weighted scans acquired at 3 T) were processed using the HCP minimal preprocessing pipeline (version 3.22.0; Glasser et al., 2013), which includes gradient nonlinearity correction via *gradunwarp*. Both T_1 and T_2 data were used to generate white matter and pial surface models using FreeSurfer (version 5.3.0; Fischl, 2012). We then removed non-brain regions from the T_1 data using the *3dSkullStrip* command from AFNI (version 18.2.04; Cox, 1996), followed by correcting for inhomogeneities in the intensity profile of gray matter and white matter voxels using AFNI's *3dUnifize*.

FMRI processing

Our fMRI data processing pipeline is summarized in Supplemental Figure 1, and began with a few simple quality control (QC) assessments. This was performed in an automated fashion using a custom python script. For each fMRI session, we first determined whether behavioral and fMRI data sets were complete (i.e., all data files were present in the expected locations), whether scans were acquired in the expected order, and whether any scans were repeated. We also determined whether date and time stamps in behavioral and fMRI data matched. For data sets that passed the QC checks above, we automatically generated shell scripts for data processing, the steps for which are described below. Data sets that failed one or both QC checks were flagged for manual intervention and held out of automated processing.

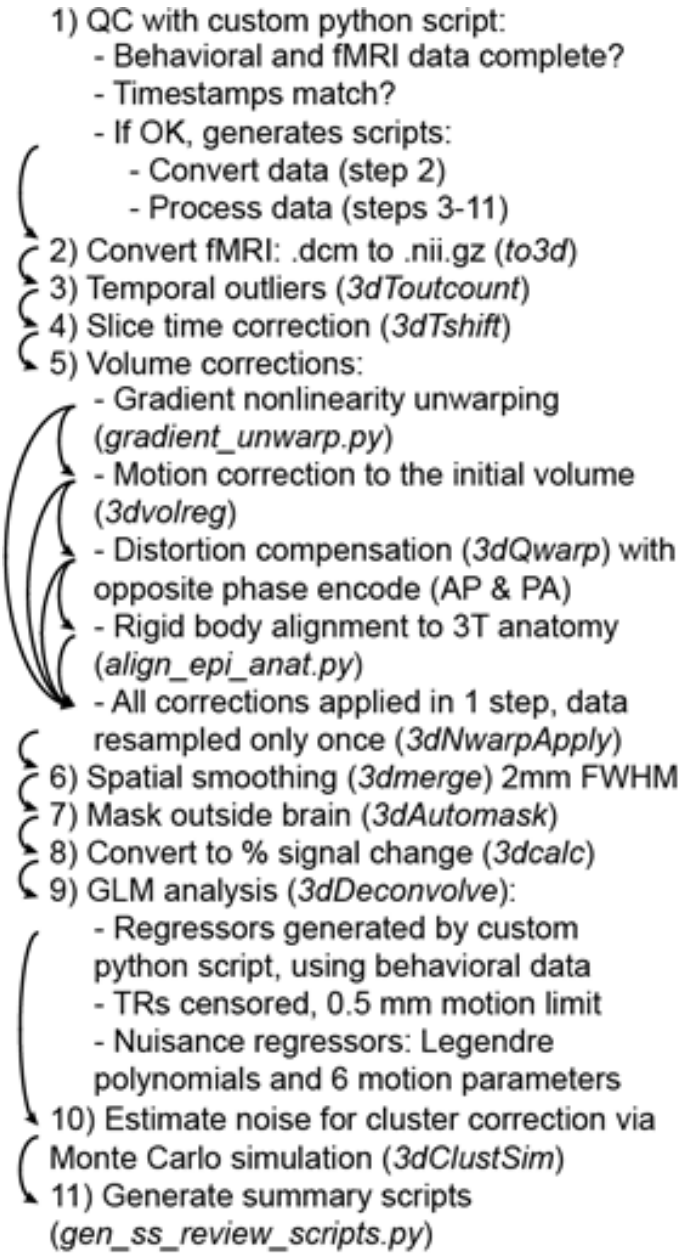

Supplemental Figure 1. Our AFNI-based data processing pipeline. Numbers and arrows indicate sequential data processing steps. Function names are given in italics.

The first step in our fMRI data processing was to convert the 7T fMRI data from DICOM to compressed (g-zipped) nifti format using AFNI's *to3d* function. We identified temporal outliers in the fMRI time series data using AFNI's *3dToutcount*, which included masking out non-brain regions (via AFNI's *3dAutomask*) and de-trending the time series using 4th order Legendre polynomials. For each TR, the fraction of voxels within the mask that were flagged as outliers (based on calculating the median absolute deviation of that voxel's time series) was found. We then performed slice time correction using AFNI's *3dTshift*, with the slice timing information extracted automatically from the header.

Next, we performed geometric corrections and transformations, which included 4 steps: 1) gradient nonlinearity unwarping (*gradunwarp* version 1.0.3; github.com/Washington-University/gradunwarp), comparable to that implemented in the HCP pipeline (Glasser et al., 2013). 2) Motion correction using AFNI's *3dvolreg*, with the first AP functional scan (PRF 1) as the base. 3) Compensation for geometric distortions due to B_0 inhomogeneities using AFNI's *3dQwarp*. We used a pair of gradient echo EPI scans with opposite phase encoding directions (posterior-anterior and anterior-posterior) acquired sequentially to map the distortion. We have recently shown that this technique yielded superior distortion compensation across the whole brain within our data set, as compared to B_0 field mapping or spin echo opposite phase encoding methods (Schallmo et al., 2021). 4) Co-registration of the 7T fMRI data to the 3T T_1-weighted anatomical scan using AFNI's *align_epi_anat.py*. Here, we used a local Pearson correlation (lpc) cost function (Saad et al., 2009) and rigid-body (6-parameter) alignment. All of these corrections were calculated sequentially, but were applied to the 7T fMRI data in a single step (i.e., data were resampled only once) using AFNI's *3dNwarpApply*, in order to avoid additional blurring that would occur from multiple resampling steps.

Following geometric corrections, we performed spatial smoothing (2 mm full-width half-max [FWHM]) using AFNI's *3dmerge*. Then, non-brain regions of the fMRI data were masked out using AFNI's *3dAutomask*. We converted our fMRI data to percent signal change using AFNI's *3dcalc*.

To quantify fMRI response magnitude, we performed general linear model (GLM) analyses using AFNI's *3dDeconvolve*. This included task regressors generated in Python based on the behavioral data collected during fMRI scanning. We censored out (i.e., removed from analysis) TRs in which head motion (i.e., framewise displacement) was greater than 0.5 mm, as identified during the earlier motion correction step. Nuisance regressors included Legendre polynomials to capture low frequency signal oscillations (polynomial order was selected for each task automatically using AFNI's default, which is 1 + [number of TRs / 150]). The 6 motion parameters estimated during motion correction were also included as nuisance regressors.

Following the GLM analysis, we obtained an estimate of the spatial profile of noise in our fMRI data using Monte Carlo simulation via AFNI's *3dClustSim* (Cox et al., 2017; Eklund et al., 2016). Finally, summary scripts were generated using AFNI's *gen_ss_review_scripts.py*, which included information about the number of temporal outliers and TRs censored for excessive head motion in each fMRI scan.

MRS processing

We used a custom python script to perform some basic, automated QC assessments of our MRS data. These checks were performed separately for both the OCC and PFC VOIs in each MRS dataset. We first assessed whether or not all expected MRS data files were present, and verified that the correct number of shots (TRs) were acquired based on the number of DICOM files. Next, we verified that the VOI was correct based on automated parsing of the DICOM file header. Finally, we tabulated VOI position and orientation based on DICOM header information, as well as shim quality (water linewidth in Hz) and transmit voltage from our (manually entered) scanning notes.

We processed our MRS data using the *matspec* toolbox (github.com/romainVala/matspec) in MATLAB (versions 2014a and 2009a). First, we performed eddy current correction for both our STEAM metabolite spectra and water reference data. To correct a known artifact, we then removed the first data point from each TR in the metabolite spectrum, and replaced it with a zero at the end of the spectrum. We then performed frequency and phase correction by finding the maximum amplitude for the spectrum at each TR within a range of 1.65 - 2.25 parts per million (ppm, i.e., the *N*-acetyl aspartate peak), and adjusting the frequency for all points in the spectrum such that the frequency of this maximum was 2.01 ppm. The phase for the maximum value was adjusted to zero on each TR. TRs with known signal artifacts (e.g., due to head motion) that could not be corrected in this way were removed manually. During frequency and phase correction, 4 Hz line broadening was applied; afterward, frequency and phase adjustments were applied to the original spectra without line broadening. We repeated our frequency and phase correction procedure across three iterations to improve correction quality. In the first two iterations, corrections were performed using the absolute value of the spectral data, while in the third iteration corrections were performed using the real portion of the complex data. A small number of data sets (n = 3 in OCC and n = 5 in PFC) were manually excluded from our analyses due to artifacts observed during data processing (e.g., failed water suppression).

Concentrations for different metabolites were quantified from the MRS data for each VOI in each scanning session using LCModel version 6.3-1N (Provencher, 2001). Our basis set was derived from previous work (Marjańska et al., 2017), and included the following 18 metabolites: ascorbic acid, aspartic acid, creatine, GABA, glucose, glutamate, glutamine, glutathione, glycerophosphorylcholine, lactate, *myo*-inositol, *N*-acetyl aspartate (NAA), *N*-acetyl aspartylglutamate (NAAG), phosphocreatine, phosphorylcholine, phosphorylethanolamine, *scyllo*-inositol, taurine, as well as lipids and macromolecules. Macromolecule signals included in the basis set were obtained from inversion-recovery experiments (Behar et al., 1994) in the OCC region of 4 healthy young adults from a previous study (Marjańska et al., 2017). The Cramér-Rao Lower Bound

(CRLB) provided an estimate of the lower limit of the variance for the fit concentration values (Cavassila et al., 2001; Landheer and Juchem, 2021). We scaled metabolite concentrations (millimolar) relative to the unsuppressed water signal, after correcting for gray matter (GM), white matter (WM), and CSF content within the region of each participant's MRS VOI. For this purpose, we used previously reported values for water content in these tissue types (GM = 0.8, WM = 0.71, CSF = 0.97), and the T_1 and T_2 relaxation time constants of water within each compartment (T_1 GM = 2130 ms, T_1 WM = 1220 ms, T_1 CSF = 4425 ms, T_2 GM = 50 ms, T_2 WM = 55 ms, T_2 CSF = 141 ms), based on previous work (Marjańska et al., 2017). Tissue fractions were quantified in each VOI in each participant using individual GM and WM surface models from FreeSurfer, after alignment of the in-session T_1 anatomy (partial coverage due to MRS surface coil) to the whole-brain T_1 data acquired at 3 T (processed with FreeSurfer). T_1 and T_2 relaxation times for the various metabolites were not accounted for in our analysis, as their effects are expected to be very small given the long TR(s) and the short TE (8 ms; Marjańska et al., 2017).

Data analysis

pRF analysis

Retinotopic analyses of pRF data (demeaned and smoothed by a 2 mm kernel) were conducted in AFNI, using a pRF implementation for the AFNI distribution (see Silson et al., 2018). We created a 2D+time binary mask of the stimulus input (191 x 191 voxels) as well as a convolution reference time series for the functional data using AFNI's *3dDeconvolve* function with GAM as the response model. The AFNI model used these inputs and both Simplex and Powell algorithms to find the optimized time series/parameter sets. For each voxel, the model outputs the (*x, y*) coordinates representing the center of the receptive field, *sigma*, representing the diameter (size) of the receptive field, and R^2, the explained variance of the fit used to statistically threshold the data.

Temporal frequency functional localizer

We used AFNI's *3dDeconvolve* command to run a general linear model (GLM) analysis in order to estimate the voxelwise magnitude of the hemodynamic responses evoked by the 2 conditions: 2 Hz and 12 Hz flicker frequency. The functional ROI was defined by contrasting 2 Hz minus 12 Hz.

Functional mapping of auditory cortex

We used Fourier analysis methods (Engel, 1997) to map fMRI responses in auditory cortex to the auditory tone sweep stimuli. Since each of the 2 runs started with either an increasing tone-sweep or decreasing tone-sweep, one of the runs was time-shifted 4 frames and time-reversed so the runs could be averaged together. Then, we filtered out the lowest frequency, and the coherence and phase were calculated from the time series data in each voxel. Coherence (a value between 0 and 1 that indicates the degree of correspondence between two signals or time series) was defined as the amplitude at a frequency divided by the absolute value of the square root of the sum of squared amplitudes at all frequencies (Engel, 1997).

Functional mapping of motor cortex

For mapping motor cortex, we used AFNI's *3dDeconvolve* command to run a GLM analysis in order to estimate the voxelwise magnitude of the hemodynamic responses evoked by each of the 5 conditions: right fingers (RF), left fingers (LF), right toes (RT), left toes (LT), and Tongue. Functional ROIs for each condition were defined by contrasting the target body part with all other body parts (e.g., for RF: RF > RT + RT + LT + Tongue). For each ROI in each participant, we chose the largest cluster (or largest 2 clusters for the Tongue condition) that overlapped with precentral/paracentral gyrus as defined by that participant's FreeSurfer parcellation. The group-level ROI represents the voxels significantly modulated in at least 50% of participants for that contrast.

CSS analysis

We fit the behavioral data from our CSS psychophysical contrast discrimination task with a psychometric (Weibull) function in order to obtain discrimination thresholds (Figure 8A). Contrast increment versus accuracy data were combined across the 3 independent staircases and fit within each stimulus condition (i.e., pedestal contrast) separately, yielding 8 independent threshold estimates (evaluated at 80% accuracy). This allowed us to examine threshold-versus-contrast curves, which show a characteristic 'dipper' shape (i.e., lowest thresholds at low, non-zero pedestal contrast; Figure 8B).

Functional MRI data from our CSS task were analyzed within regions-of-interest (ROIs) in area V1. These V1 ROIs were defined using the functional localizer data (i.e., the first 90 s task condition from the first scanning run). We used a Fourier analysis (Engel, 1997; Schallmo et al., 2016) to identify voxels that responded selectively to the center > surrounding stimulus (green voxels in Figure 8C). Center-selective voxels were identified based on a coherence (a value between 0 and 1 that indicates the degree of correspondence between two signals or time series) threshold ≥ 0.2, and phase values between 7π/8 to 11π/8 (i.e., in phase with the center stimulus presentation, accounting for the delayed hemodynamic response). V1 ROIs were defined in AFNI using a cluster correction method (Cox et al., 2017; Eklund et al., 2016), with a whole-brain significance threshold of $p < 0.01$. V1 clusters were identified in each hemisphere in each individual and scanning session using a V1 anatomical mask (Wang et al., 2015) from FreeSurfer and manual inspection of the participant's functional activation map and occipital anatomy in SUMA and AFNI. We chose to use V1 anatomical masks, rather than functionally-defined masks from the pRF data, to allow our CSS and pRF data processing streams to proceed independently. V1 responses in the CSS fMRI task were quantified in terms of percent signal change using a Fourier analysis in MATLAB, based on the stimulus presentation frequency (5 cycles of target-on, target-off per 90 s stimulus condition).

COP analyses

Our analyses of the psychophysical and fMRI data from the COP task matched that in the CSS task above, with the following differences. Data from the 3 staircases in each block were combined for fitting purposes, yielding 2 independent threshold estimates for contour jitter versus accuracy (1 in each block; Figure 9A). Thresholds were assessed at 70% accuracy in the COP psychophysical task. This was done in order to enable quantification of thresholds for participants with relatively low ceiling performance (i.e., contour discrimination accuracy ~80% for aligned contours with 0° jitter). V1 ROIs in the COP task were defined using a Fourier analysis (contour > blank), with a correlation threshold ≥ 0.3 and phase values 0 to 3π/8 and 15π/8 to 2π (Figure 9C). V1 responses in the COP fMRI task were quantified in terms of percent signal change (i.e., beta weights) using a GLM analysis in AFNI (see FMRI Processing in Supplemental Methods).

SFM analysis

Switch rates (in Hz) for bi-stable percepts were quantified by dividing the number of switches reported in each 2 min block and dividing by 120 sec, and then averaging across all 5 bi-stable stimulus blocks. Repeated responses indicating the same perceived direction were ignored.

MRS analysis

In order to visualize average MRS VOI positions in OCC and PFC, we transformed binary VOI masks from the individual participant space to MNI space using FreeSurfer's *mri_convert* function and the *talairach.xfm* from each participant. We then computed the voxel-wise average VOI position using AFNI's *3dMean*. Average VOIs were visualized on a canonical brain image in AFNI (Figure 12B & D), thresholded at > 30% overlap across participants. MRS results from LCModel were analyzed in MATLAB.

Supplemental results

Supplemental Table 1. Demographics, cognitive, and symptom measures for PwPP, by diagnostic group. Data are presented as mean (standard deviation), unless otherwise noted. Racial and ethnic designations (as defined by the National Institute of Health) are abbreviated as follows: A = Asian or Pacific Islander, B = Black (not of Hispanic origin), H = Hispanic, N = Native American or Alaskan Native, W = White (not of Hispanic origin), M = More than 1 race or ethnicity, or other. Visual acuity was assessed with a Snellen eye chart (Snellen, 1862); the decimal fraction is reported (e.g., 0.5 indicates 20/40). Visual contrast sensitivity was assessed with the Mars Letter Contrast Sensitivity test (Arditi, 2005). Estimated IQ was assessed using the Wechsler Adult Intelligence Scale (WAIS-IV; Wechsler, 2008). BACS = Brief Assessment of Cognition in Schizophrenia, Z-score (Keefe et al., 1999), BPRS = Brief Psychiatric Rating Scale (Ventura et al., 2000), SGI = Sensory Gating Inventory (Hetrick et al., 2012), SPQ = Schizotypal Personality Questionnaire (Raine, 1991), PID-5 psychoticism = psychoticism factor from the Personality Inventory for DSM-5 (Krueger et al., 2012), SANS = Scale for the Assessment of Negative Symptoms (Andreasen, 1982), SAPS = Scale for the Assessment of Positive Symptoms (Andreasen, 1984). Diagnoses were based on the Structured Clinical Interview for DSM-IV-TR disorders (SCID; First, 1997). Data collected at repeat scans were not included here. The statistics column shows the test statistic and *p*-value for differences across all three groups in each measure. For measures where normality and / or homogeneity of variance were not observed, non-parametric Kruskal-Wallis tests (X^2-values) were used in place of analyses of variance (*F*-values).

	Schizophrenia, n = 36	**Schizoaffective disorder**, n = 10	**Bipolar disorder**, n = 20	**Statistics**
Age in years	39.9 (11.1)	37.5 (12.9)	36.3 (12.0)	$F_{(2,63)} = 0.66$, $p = 0.5$
Sex assigned at birth	11 F, 25 M	4 F, 6 M	16 F, 4 M	$X^2_{(2)} = 12.8$, $p = 0.002$
Race / ethnicity (%; A / B / H / N / W / M)	5.6 / 22.2 / 2.8 / 0 / 66.7 / 2.8	10.0 / 10.0 / 10.0 / 0 / 70.0 / 0	0 / 5.0 / 0 / 0 / 90 / 5.0	-
Education (years)	13.5 (2.0)	13.3 (2.2)	16.0 (1.9)	$F_{(2,63)} = 10.5$, $p = 1 \times 10^{-4}$
Visual acuity (decimal fraction)	0.83 (0.25)	1.14 (1.10)	1.02 (0.45)	$F_{(2,44)} = 1.11$, $p = 0.3$
Visual contrast sensitivity	1.79 (0.08)	1.76 (0.07)	1.81 (0.04)	$F_{(2,63)} = 1.72$, $p = 0.19$
Estimated IQ	93.4 (9.8)	96.4 (11.1)	104.2 (8.9)	$F_{(2,63)} = 7.95$, $p = 8 \times 10^{-4}$
BACS	-0.79 (0.70)	-0.75 (0.56)	-0.39 (0.67)	$F_{(2,62)} = 2.40$, $p = 0.10$
BPRS	45.0 (11.2)	46.1 (6.6)	35.8 (8.6)	$X^2_{(2)} = 12.8$, $p = 0.002$
SGI	72.1 (27.1)	82.9 (30.3)	57.6 (30.5)	$X^2_{(2)} = 5.04$, $p = 0.081$
SPQ	33.2 (14.5)	38.3 (13.7)	21.5 (12.6)	$X^2_{(2)} = 11.5$, $p = 0.003$
PID-5 psychoticism	1.28 (0.63)	1.31 (0.58)	0.88 (0.58)	$X^2_{(2)} = 6.37$,

				$p = 0.042$
SAPS	6.19 (4.73)	5.60 (3.06)	1.90 (2.43)	$X^2_{(2)} = 12.7$, $p = 0.002$
SANS	8.03 (3.32)	5.30 (2.71)	3.25 (3.42)	$X^2_{(2)} = 19.8$, $p = 5 \times 10^{-5}$
Days between 3 T and 7 T scans	222 (298)	256 (367)	267 (319)	-
# of 7 T return visits	18	5	16	-
Days between 7 T repeat scans	222 (306)	257 (268)	288 (345)	-

Supplemental Table 2. Number of data sets collected under the protocols we refer to as 7T-A and 7T-B / Z in each experiment and participant group. Note that the number of unique participants is lower than the total number of data sets, as some participants returned for a repeat scan, as reported in Table 1. Psych. = psychophysics.

		Controls	**Relatives**	**PwPP**
7T-A	CSS psych.	10	0	5
	COP psych.	17	0	5
	COP fMRI	12	0	3
7T-B / Z	CSS psych.	33	44	100
	COP psych.	34	44	100
	COP fMRI	33	39	74

Supplemental Table 3. Longitudinal variability of clinical measures. Data presented are from n = 38 PwPP who completed two scanning sessions (e.g., 7T-B & 7T-Z) and for whom BPRS (Ventura et al., 2000), SANS (Andreasen, 1982), and SAPS (Andreasen, 1984) data were acquired during both visits. Rows show data for these three measures, columns show the metrics quantifying change between scans after taking the absolute value (abs.) of the difference between data from scan 1 and scan 2, as well as statistics comparing data from scans 1 & 2. No significant changes (i.e., no consistent increases or decreases) in BPRS, SANS, or SAPS scores were observed between sessions. *SD* = standard deviation.

	Mean abs. change	*SD* abs. change	Median abs. change	Statistics
BPRS total score	6.37	5.01	4.5	$t_{(37)} = 0.56$, $p = 0.6$
SANS total global score	2.37	2.42	1.5	$t_{(37)} = -1.37$, $p = 0.2$
SAPS total global score	2.00	1.93	2	$t_{(37)} = 0.46$, $p = 0.6$

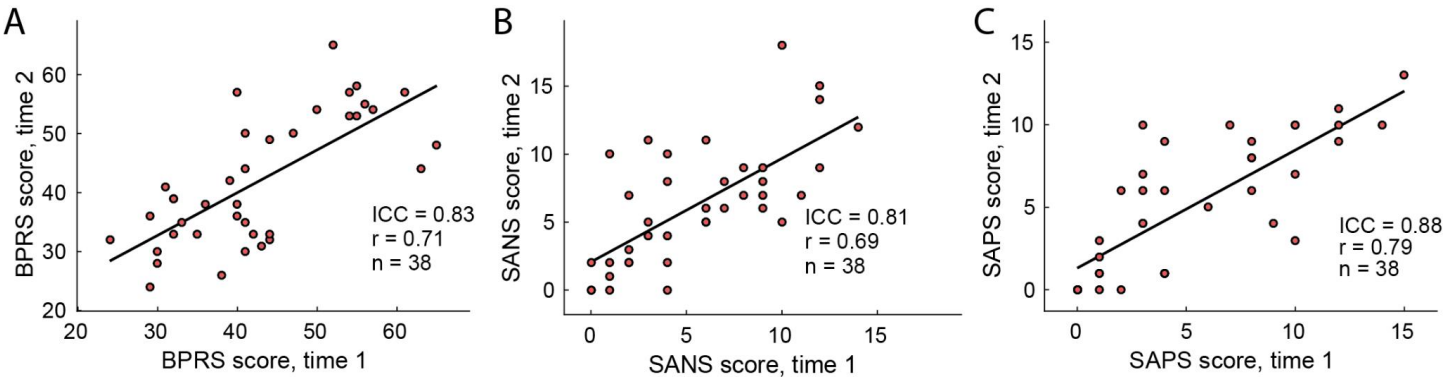

Supplemental Figure 2. Scatter plots of clinical measures over time. Data presented are from n = 38 PwPP who completed two scanning sessions (e.g., 7T-B & 7T-Z) and for whom BPRS (Ventura et al., 2000), SANS (Andreasen, 1982), and SAPS (Andreasen, 1984) data were acquired during both visits. A) BPRS total score, B) SANS total global score, C) SAPS total global score. X-axes show data from scanning session 1, y-axes show data from session 2. Black line shows the linear trend. ICC = intraclass correlation coefficient, ICC(3,k), (Koo and Li, 2016); r = Pearson's r-value.

Supplemental Table 4. Number of data sets with eye tracking data. Note that the number of unique participants is lower than the total number of data sets, as some participants returned for a repeat scan, as reported in Table 1.

		Controls	**Relatives**	**PwPP**
Psychophysics	CSS	24	33	81
	COP	24	34	81
	SFM	26	35	85
fMRI	pRF	19	20	42
	CSS	18	19	40
	COP	13	17	34

Supplemental Table 5. Statistical comparisons of psychophysics and fMRI data quality metrics between groups. For visualizations of these data, see Supplemental Figure 3, Supplemental Figure 4, & Supplemental Figure 5. As most metrics were not normally distributed, Kruskal-Wallis nonparametric 1-way ANOVAs were used to quantify between-group differences.

	pRF	**CSS**	**COP**	**SFM**
Psychophysical catch trial accuracy	-	$X^2_{(2)} = 8.99$, $p = 0.011$	$X^2_{(2)} = 4.30$, $p = 0.12$	$X^2_{(2)} = 2.37$, $p = 0.3$
fMRI head motion (# TRs censored)	$X^2_{(2)} = 7.71$, $p = 0.021$	$X^2_{(2)} = 11.8$, $p = 0.003$	$X^2_{(2)} = 14.4$, $p = 8 \times 10^{-4}$	-
fMRI behavioral responses (% of trials)	$X^2_{(2)} = 10.1$, $p = 0.006$	$X^2_{(2)} = 6.08$, $p = 0.048$	$X^2_{(2)} = 3.45$, $p = 0.18$	-
fMRI head motion (avg. per TR)	$X^2_{(2)} = 8.99$, $p = 0.011$	$X^2_{(2)} = 10.1$, $p = 0.006$	$X^2_{(2)} = 10.0$, $p = 0.007$	-
fMRI temporal outliers (% of voxels per TR)	$X^2_{(2)} = 6.87$, $p = 0.032$	$X^2_{(2)} = 11.1$, $p = 0.004$	$X^2_{(2)} = 10.8$, $p = 0.005$	-

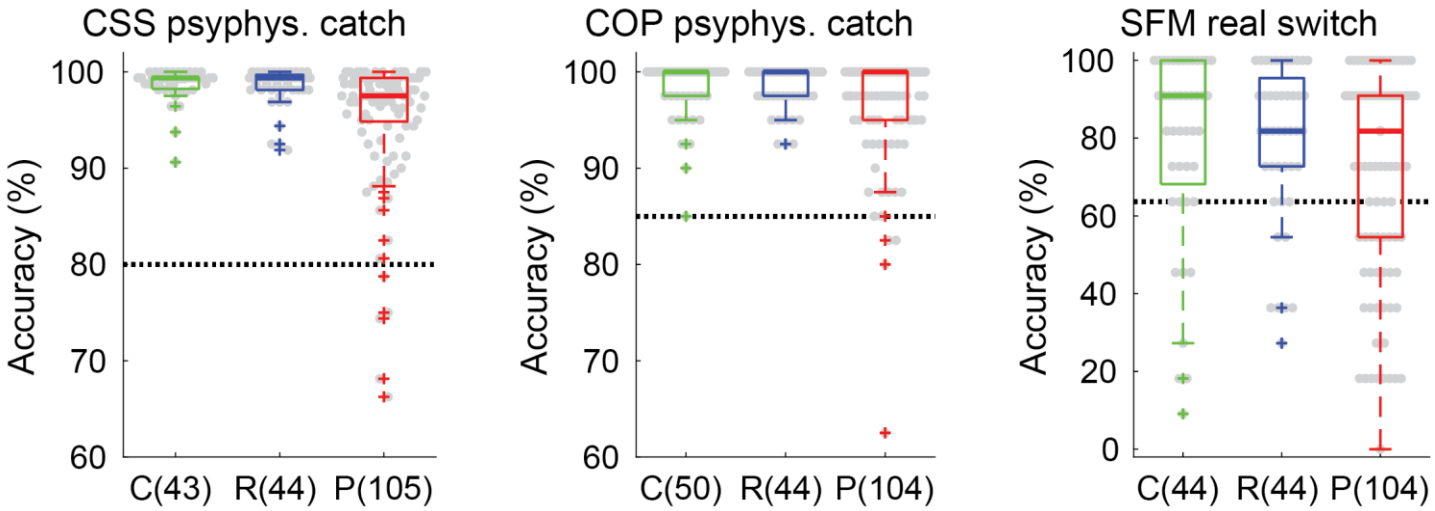

Supplemental Figure 3. Psychophysical data quality checks across groups and experiments. Panels show catch trial accuracy from the CSS (left) and COP (middle) psychophysical (psyphys.) tasks, as well as accuracy for responses made in < 4 s in the SFM real switch psychophysical task (right). The number of data sets (not unique individuals) per group and experiment are shown in parentheses. C = healthy controls (green), R = first-degree biological relatives (blue), P = people with psychotic psychopathology (red). Thick lines show group medians, boxes show 25-75%, whiskers show 1.5 x interquartile range, dots show individual data points, dashed black lines show data quality thresholds.

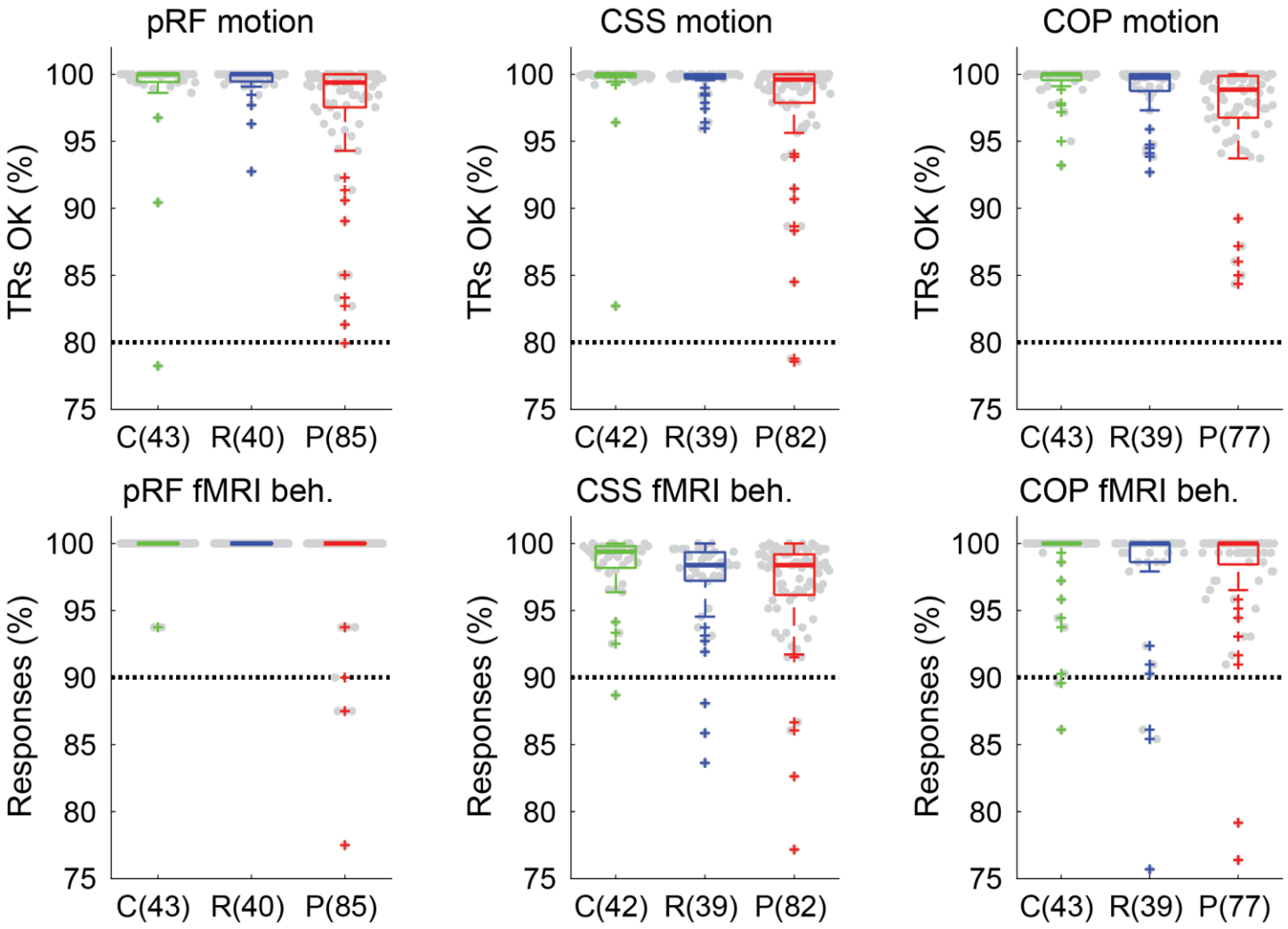

Supplemental Figure 4. FMRI data quality checks across groups and experiments. Top row shows the proportion of TRs with < 0.5 mm of head motion (i.e., framewise displacement) in the pRF (left), CSS (middle), and COP (right) fMRI tasks. Bottom row shows the same, but for the proportion of trials in which a behavioral (beh.) response was recorded (regardless of accuracy). The number of data sets (not unique individuals) per group and experiment are shown in parentheses. C = healthy controls (green), R = first-degree biological relatives (blue), P = people with psychotic psychopathology (red). Thick lines show group medians, boxes show 25-75%, whiskers show 1.5 x interquartile range, dots show individual data points, dashed black lines show data quality thresholds. Note that in the pRF motion plot (top left), an outlier data point from a single PwPP is not shown, in order to better visualize the distributions of the other data points. The same is true for COP motion (top right; 1 control and 1 PwPP), pRF fMRI behavior (bottom left; 2 controls, 4 PwPP), and COP fMRI behavior (bottom right; 1 relative, 2 PwPP).

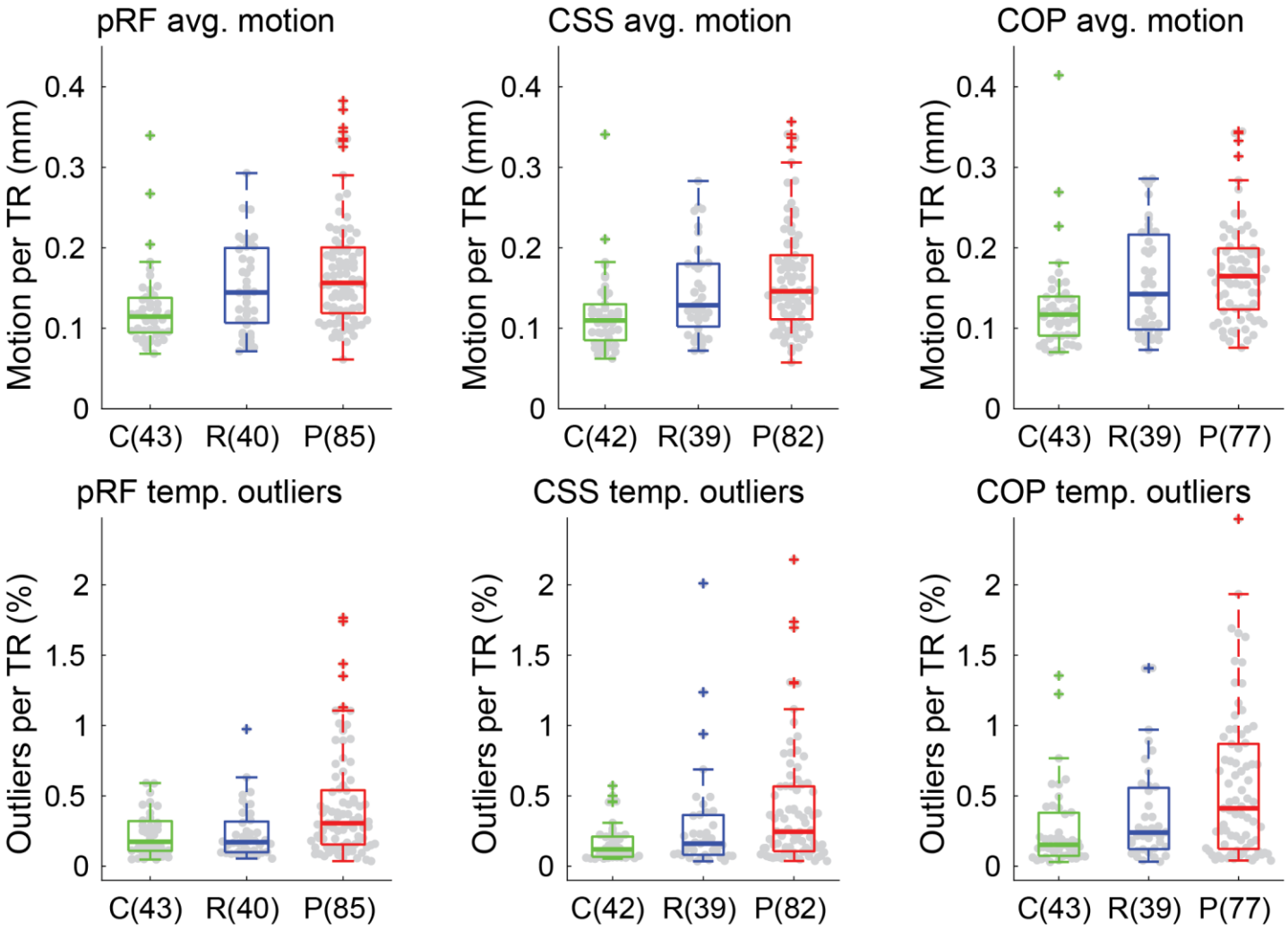

Supplemental Figure 5. Motion per TR and temporal outliers per TR, across groups and fMRI experiments. Top row shows the average (avg.) head motion per TR (i.e., framewise displacement) for the pRF (left), CSS (middle), and COP (right) fMRI tasks. The bottom row shows the same, but for the percent of voxels labeled as temporal (temp.) outliers per TR. The number of data sets (not unique individuals) per group and experiment are shown in parentheses. C = healthy controls (green), R = first-degree biological relatives (blue), P = people with psychotic psychopathology (red). Thick lines show group medians, boxes show 25-75%, whiskers show 1.5 x interquartile range, dots show individual data points. Note that in the COP average motion plot (top right), an outlier data point from a single PwPP is not shown, in order to better visualize the distributions of the other data points.

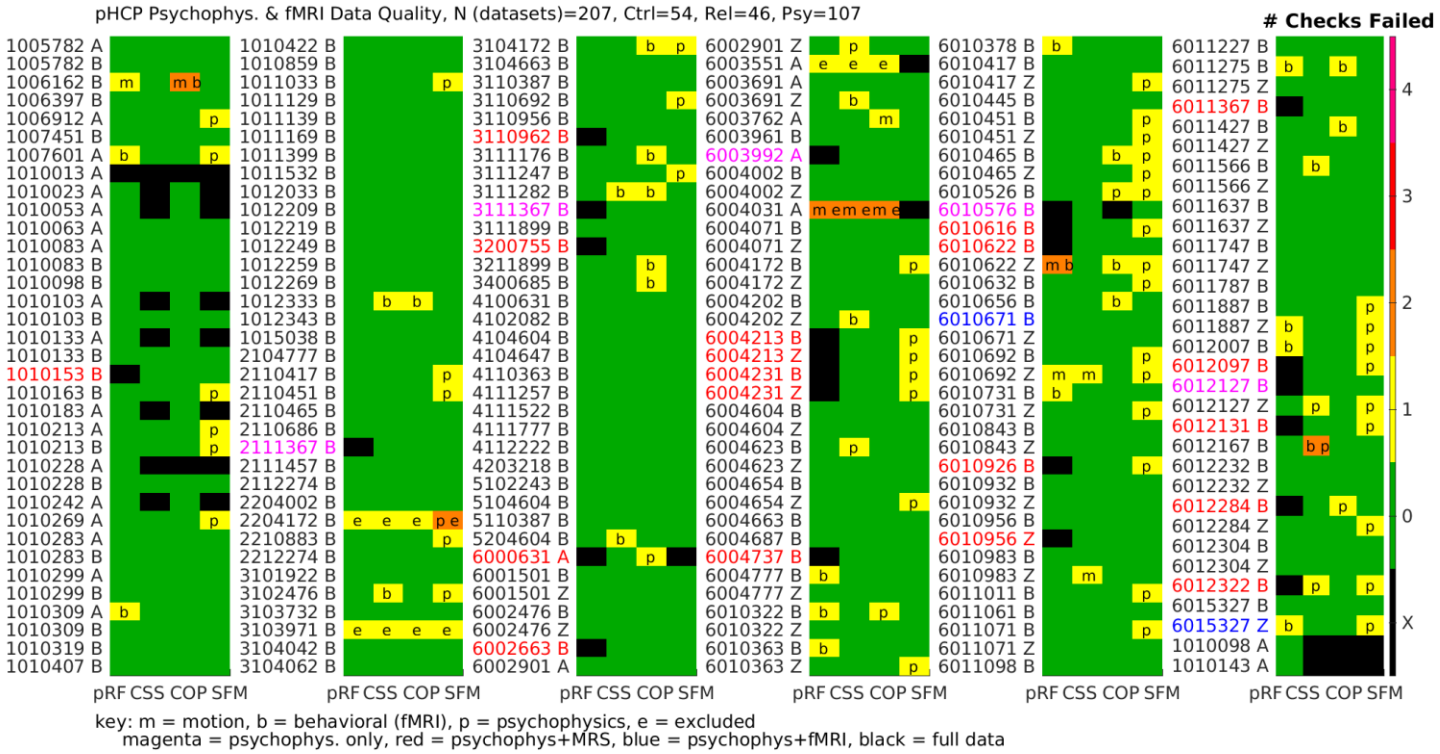

Supplemental Figure 6. Psychophysics and fMRI data quality detailed summary. Rows show individual data sets labeled by participant ID number and protocol (A, B, or Z). The font color for the row labels indicates whether there is a full data set (black), psychophysics & fMRI only (blue), psychophysics & MRS only (red), or psychophysics only (magenta). Columns show data for the 4 different visual paradigms (pRF = population receptive field modeling, CSS = contrast surround suppression, COP = contour object perception, SFM = structure-from-motion). Colors within the table show the number of data quality checks that were failed (black = missing data). Letters within the table indicate which checks were failed (m = motion, b = fMRI behavioral task, p = psychophysical catch trials, e = excluded data). Note that data sets that were collected but subsequently excluded (e) appear here for the sake of completeness, but are not included elsewhere in the manuscript unless otherwise noted.

Supplemental Table 6. Statistical comparisons of MRS data quality metrics between groups. For visualization of these data, see Supplemental Figure 7. Kruskal-Wallis nonparametric 1-way ANOVAs were used to quantify between-group differences.

	OCC	**PFC**
H_2O linewidth	$X^2_{(2)} = 1.12$, $p = 0.6$	$X^2_{(2)} = 3.02$, $p = 0.2$
LCModel linewidth	$X^2_{(2)} = 3.24$, $p = 0.2$	$X^2_{(2)} = 2.33$, $p = 0.3$
SNR	$X^2_{(2)} = 6.87$, $p = 0.032$	$X^2_{(2)} = 2.08$, $p = 0.4$

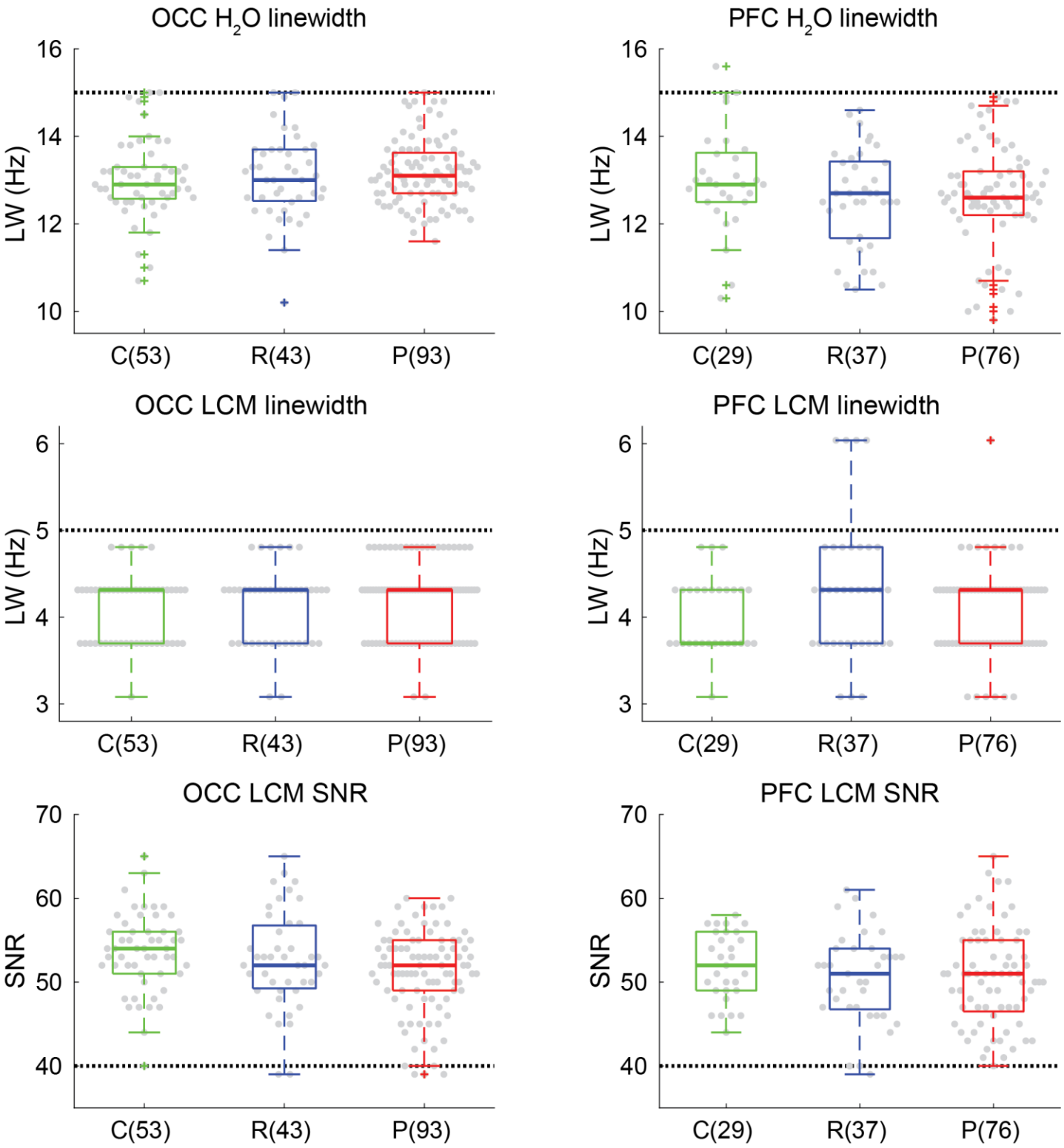

Supplemental Figure 7. MRS data quality checks across groups and experiments. Top row shows the linewidth of water (H_2O) in the OCC (left) and PFC (right) VOIs. Middle row shows the same, but for the linewidth of the fitted spectrum from LCModel (LCM), whereas the bottom row shows SNR from LCModel. The number of data sets (not unique individuals) per group and experiment are shown in parentheses. C = healthy controls (green), R = first-degree biological relatives (blue), P = people with psychotic psychopathology (red). Thick lines show group medians, boxes show 25-75%, whiskers show 1.5 x interquartile range, dots show individual data points, dashed black lines show data quality thresholds. Participants with missing quality data (e.g., linewidth of water was not recorded during scanning) are not shown. Note that in the PFC H_2O linewidth plot (top right), outlier data points from two PwPP are not shown, in order to better visualize distributions of the other data points. The same is true for PFC LCModel SNR (bottom right; 1 relative, 2 PwPP).

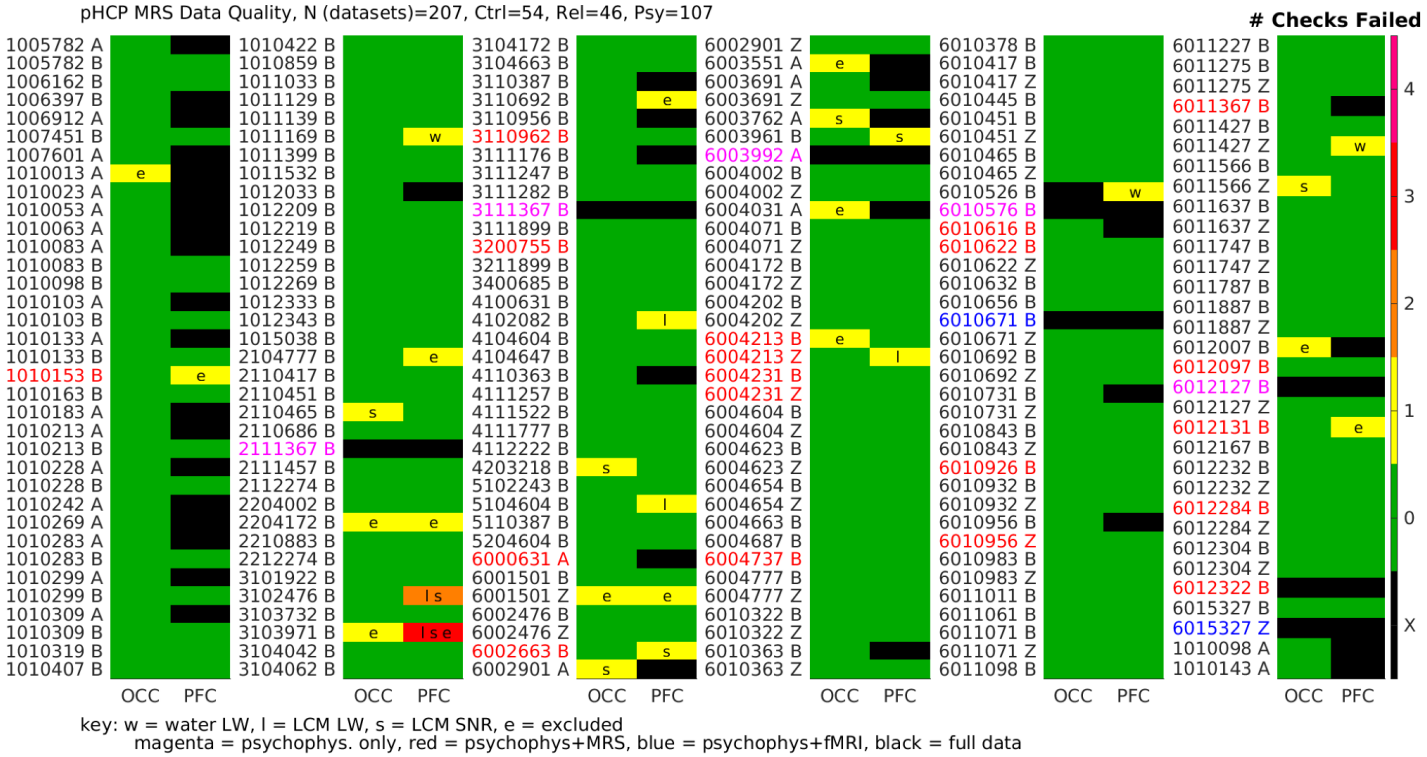

Supplemental Figure 8. MRS data quality detailed summary. Rows show individual data sets labeled by participant ID number and protocol (A, B, or Z). The font color for the row labels indicates whether there is a full data set (black), psychophysics & fMRI only (blue), psychophysics & MRS only (red), or psychophysics only (magenta). Columns show data for the 2 different MRS VOIs (OCC = occipital cortex, PFC = prefrontal cortex). Colors within the table show the number of data quality checks that were failed (black = missing data). Letters within the table indicate which checks were failed (w = linewidth of water, l = linewidth from LCModel, s = SNR from LCModel, e = excluded data). Note that data sets that were collected but subsequently excluded (e) appear here for the sake of completeness, but are not included elsewhere in the manuscript unless otherwise noted.

Supplemental References

Albrecht, D.G., Hamilton, D.B., 1982. Striate cortex of monkey and cat: Contrast response function. Journal of Neurophysiology 48, 217-237.

Altmann, C., Bülthoff, H., Kourtzi, Z., 2003. Perceptual organization of local elements into global shapes in the human visual cortex. Current Biology 13, 342-349.

Anderson, E.J., Tibber, M.S., Schwarzkopf, D.S., Shergill, S.S., Fernandez-Egea, E., Rees, G., Dakin, S.C., 2017. Visual population receptive fields in people with schizophrenia have reduced inhibitory surrounds. The Journal of Neuroscience 37, 1546-1556.

Andreasen, N.C., 1982. Negative symptoms in schizophrenia: Definition and reliability. Archives of general psychiatry 39, 784-788.

Andreasen, N.C., 1984. Scale for the assessment of positive symptoms. University of Iowa, Iowa City, IA.

Angelucci, A., Bressloff, P.C., 2006. Contribution of feedforward, lateral, and feedback connections to the classical receptive field center and extra-classical receptive field surround of primate V1 neurons. In: Martinez-Conde, M., Martinez, Alonso, & Tse (Ed.), Progress in Brain Research, pp. 93-120.

Arditi, A., 2005. Improving the design of the letter contrast sensitivity test. Investigative Opthalmology & Visual Science 46, 2225.

Bair, W., Cavanaugh, J.R., Movshon, J.A., 2003. Time course and time-distance relationships for surround suppression in macaque V1 neurons. The Journal of Neuroscience 23, 7690.

Barch, D.M., Carter, C.S., Dakin, S.C., Gold, J., Luck, S.J., MacDonald, A.W., Ragland, J.D., Silverstein, S., Strauss, M.E., 2012. The clinical translation of a measure of gain control: The contrast-contrast effect task. Schizophrenia Bulletin 38, 135-143.

Bauer, R., Heinze, S., 2002. Contour integration in striate cortex. Experimental Brain Research 147, 145-152.

Behar, K.L., Rothman, D.L., Spencer, D.D., Petroff, C., 1994. Analysis of macromolecule resonances in 1H NMR spectra of human brain. Magnetic Resonance in Medicine 32, 294-302.

Bennett, D., Dluzniak, A., Cropper, S.J., Partos, T., Sundram, S., Carter, O., 2016. Selective impairment of global motion integration, but not global form detection, in schizophrenia and bipolar affective disorder. Schizophrenia Research: Cognition 3, 11-14.

Boynton, G.M., Demb, J.B., Glover, G.H., Heeger, D.J., 1999. Neuronal basis of contrast discrimination. Vision Research 39, 257-269.

Butler, P.D., Martinez, A., Foxe, J.J., Kim, D., Zemon, V., Silipo, G., Mahoney, J., Shpaner, M., Jalbrzikowski, M., Javitt, D.C., 2007. Subcortical visual dysfunction in schizophrenia drives secondary cortical impairments. Brain 130, 417.

Butler, P.D., Silverstein, S., Dakin, S.C., 2008. Visual perception and its impairment in schizophrenia. Biological Psychiatry 64, 40-47.

Butler, P.D., Zemon, V., Schechter, I., Saperstein, A.M., Hoptman, M.J., Lim, K.O., Revheim, N., Silipo, G., Javitt, D.C., 2005. Early-stage visual processing and cortical amplification deficits in schizophrenia. Archives of general psychiatry 62, 495.

Cai, Y.-C., Zhou, T., Chen, L., 2008. Effects of binocular suppression on surround suppression. Journal of Vision 8, 9.

Calderone, D.J., Martinez, A., Zemon, V., Hoptman, M.J., Hu, G., Watkins, J.E., Javitt, D.C., Butler, P.D., 2013. Comparison of psychophysical, electrophysiological, and fMRI assessment of visual contrast responses in patients with schizophrenia. NeuroImage 67, 153-162.

Carandini, M., Heeger, D.J., 2012. Normalization as a canonical neural computation. Nature Reviews Neuroscience 13, 51-62.

Carter, O., Bennett, D., Nash, T., Arnold, S., Brown, L., Cai, R.Y., Allan, Z., Dluzniak, A., McAnally, K., Burr, D., Sundram, S., 2017. Sensory integration deficits support a dimensional view of psychosis and are not limited to schizophrenia. Translational Psychiatry 7, e1118.

Cavanaugh, J.R., Bair, W., Movshon, J.A., 2002. Selectivity and spatial distribution of signals from the receptive field surround in macaque V1 neurons. Journal of Neurophysiology 88, 2547-2556.

Cavassila, S., Deval, S., Huegen, C., van Ormondt, D., Graveron-Demilly, D., 2001. Cramér–Rao bounds: an evaluation tool for quantitation. NMR Biomed. 14, 278-283.

Chen, C.-C., 2014. Partitioning two components of BOLD activation suppression in flanker effects. Frontiers in Neuroscience 8, 149.

Chen, Y., Bidwell, L.C., Holzman, P.S., 2005. Visual motion integration in schizophrenia patients, their first-degree relatives, and patients with bipolar disorder. Schizophrenia Research 74, 271-281.

Chubb, C., Sperling, G., Solomon, J.A., 1989. Texture interactions determine perceived contrast. Proceedings of the National Academy of Sciences 86, 9631-9635.

Cox, R.W., 1996. AFNI: software for analysis and visualization of functional magnetic resonance neuroimages. Computers and Biomedical research 29, 162-173.

Cox, R.W., Chen, G., Glen, D.R., Reynolds, R.C., Taylor, P.A., 2017. FMRI clustering in AFNI: False-positive rates redux. Brain Connectivity 7.

Dakin, S., Carlin, P., Hemsley, D., 2005. Weak suppression of visual context in chronic schizophrenia. Current Biology 16, R822-R824.

Demro, C., Mueller, B.A., Kent, J.S., Burton, P.C., Olman, C.A., Schallmo, M.-P., Lim, K.O., Sponheim, S.R., 2021. The psychosis human connectome project: An overview. NeuroImage 241, 118439.
Dymerska, B., Poser, B.A., Barth, M., Trattnig, S., Robinson, S.D., 2018. A method for the dynamic correction of B0 - related distortions in single-echo EPI at 7 T. NeuroImage 168, 321-331.
Eklund, A., Nichols, T.E., Knutsson, H., 2016. Cluster failure: Why fMRI inferences for spatial extent have inflated false-positive rates. Proceedings of the National Academy of Sciences 113, 7900-7905.
Emir, U.E., Auerbach, E.J., Moortele, P.-F.V.D., Marjańska, M., Uğurbil, K., Terpstra, M., Tkáč, I., Öz, G., 2012. Regional neurochemical profiles in the human brain measured by ^{1}H MRS at 7 T using local B_1 shimming: Single-voxel MRS at 7 T with transceiver array coil. NMR in Biomedicine 25, 152-160.
Engel, S., 1997. Retinotopic organization in human visual cortex and the spatial precision of functional MRI. Cerebral Cortex 7, 181-192.
Farnsworth, D., 1943. The Farnsworth-Munsell 100-Hue and Dichotomous Tests for Color Vision. Journal of the Optical Society of America 33, 568.
Fernandes, T.P., Silverstein, S.M., Almeida, N.L., Santos, N.A., 2019. Visual impairments in type 1 bipolar disorder. The World Journal of Biological Psychiatry 20, 790-798.
First, M.B., 1997. User's guide for the structured clinical interview for DSM-IV axis I disorders SCID-I: clinician version. American Psychiatric Publishing, Inc.
Fischl, B., 2012. FreeSurfer. NeuroImage 62, 774-781.
Foss-Feig, J.H., Adkinson, B.D., Ji, J.L., Yang, G., Srihari, V.H., McPartland, J.C., Krystal, J.H., Murray, J.D., Anticevic, A., 2017. Searching for cross-diagnostic convergence: Neural mechanisms governing excitation and inhibition balance in schizophrenia and autism spectrum disorders. Biological Psychiatry 81, 848-861.
Fox, R., 1965. Rate of binocular rivalry alternation in psychotic and nonpsychotic patients. Journal of Abnormal Psychology 70, 34-37.
Glasser, M.F., Smith, S.M., Marcus, D.S., Andersson, J.L.R., Auerbach, E.J., Behrens, T.E.J., Coalson, T.S., Harms, M.P., Jenkinson, M., Moeller, S., Robinson, E.C., Sotiropoulos, S.N., Xu, J., Yacoub, E., Ugurbil, K., Van Essen, D.C., 2016. The Human Connectome Project's neuroimaging approach. Nature neuroscience 19, 1175-1187.
Glasser, M.F., Sotiropoulos, S.N., Wilson, J.A., Coalson, T.S., Fischl, B., Andersson, J.L., Xu, J., Jbabdi, S., Webster, M., Polimeni, J.R., Van Essen, D.C., Jenkinson, M., 2013. The minimal preprocessing pipelines for the Human Connectome Project. NeuroImage 80, 105-124.
Godlewska, B.R., Clare, S., Cowen, P.J., Emir, U.E., 2017. Ultra-High-Field Magnetic Resonance Spectroscopy in Psychiatry. Frontiers in Psychiatry 8, 123.
Grove, T.B., Yao, B., Mueller, S.A., McLaughlin, M., Ellingrod, V.L., McInnis, M.G., Taylor, S.F., Deldin, P., Tso, I.F., 2018. A Bayesian model comparison approach to test the specificity of visual integration impairment in schizophrenia or psychosis. Psychiatry Research 265, 271-278.
Henning, A., 2018. Proton and multinuclear magnetic resonance spectroscopy in the human brain at ultra-high field strength: A review. NeuroImage 168, 181-198.
Hetrick, W.P., Erickson, M.A., Smith, D.A., 2012. Phenomenological dimensions of sensory gating. Schizophrenia Bulletin 38, 178-191.
Joo, S.J., Boynton, G.M., Murray, S.O., 2012. Long-range, pattern-dependent contextual effects in early human visual cortex. Current Biology 22, 781-786.
Katzner, S., Busse, L., Carandini, M., 2011. $GABA_A$ inhibition controls response gain in visual cortex. The Journal of Neuroscience 31, 5931-5941.
Keane, B.P., Barch, D.M., Mill, R.D., Silverstein, S.M., Krekelberg, B., Cole, M.W., 2021. Brain network mechanisms of visual shape completion. NeuroImage 236, 118069.
Keane, B.P., Joseph, J., Silverstein, S.M., 2014. Late, not early, stages of Kanizsa shape perception are compromised in schizophrenia. Neuropsychologia 56, 302-311.
Keane, B.P., Paterno, D., Kastner, S., Krekelberg, B., Silverstein, S.M., 2018. Intact illusory contour formation but equivalently impaired visual shape completion in first- and later-episode schizophrenia. Journal of Abnormal Psychology 128, 57-68.
Keane, B.P., Paterno, D., Kastner, S., Silverstein, S.M., 2016. Visual integration dysfunction in schizophrenia arises by the first psychotic episode and worsens with illness duration. Journal of Abnormal Psychology 125, 543-549.
Keefe, R.S.E., Goldberg, T.E., Harvey, P.D., Gold, J., Poe, M.P., Coughenour, L., 1999. Brief assessment of cognition in schizophrenia. Schizophrenia Research.
Keri, S., Antal, A., Szekeres, G., Benedek, G., Janka, Z., 2002. Spatiotemporal visual processing in schizophrenia. Journal of Neuropsychiatry and Clinical Neurosciences 14, 190.
Koo, T.K., Li, M.Y., 2016. A guideline of selecting and reporting intraclass correlation coefficients for reliability research. Journal of Chiropractic Medicine 15, 155-163.
Krueger, R.F., Derringer, J., Markon, K.E., Watson, D., Skodol, A.E., 2012. Initial construction of a maladaptive personality trait model and inventory for DSM-5. Psychological Medicine 42, 1879-1890.
Lalor, E.C., De Sanctis, P., Krakowski, M.I., Foxe, J.J., 2012. Visual sensory processing deficits in schizophrenia: Is there anything to the magnocellular account? Schizophrenia Research 139, 246-252.

Landheer, K., Juchem, C., 2021. Are Cramér-Rao lower bounds an accurate estimate for standard deviations in in vivo magnetic resonance spectroscopy? NMR in Biomedicine 34, e4521.
Legge, G.E., Foley, J.M., 1980. Contrast masking in human vision. Journal of the Optical Society of America 70, 1458-1471.
Li, W., Piëch, V., Gilbert, C., 2006. Contour saliency in primary visual cortex. Neuron 50, 951-962.
Li, W., Piëch, V., Gilbert, C.D., 2008. Learning to link visual contours. Neuron 57, 442-451.
Linares, D., Amoretti, S., Marin-Campos, R., Sousa, A., Prades, L., Dalmau, J., Bernardo, M., Compte, A., 2020. Spatial suppression and sensitivity for motion in schizophrenia. Schizophrenia Bulletin Open 1, sgaa045.
Lisman, J., 2012. Excitation, inhibition, local oscillations, or large-scale loops: What causes the symptoms of schizophrenia? Current Opinion in Neurobiology 22, 537-544.
Loffler, G., 2008. Perception of contours and shapes: Low and intermediate stage mechanisms. Vision Research 48, 2106-2127.
Long, J.D., Brekke, J.S., 1999. Longitudinal factor structure of the brief psychiatric rating scale in schizophrenia. Psychological Assessment 11, 498-506.
Marjańska, M., McCarten, J.R., Hodges, J., Hemmy, L.S., Grant, A., Deelchand, D.K., Terpstra, M., 2017. Region-specific aging of the human brain as evidenced by neurochemical profiles measured noninvasively in the posterior cingulate cortex and the occipital lobe using 1H magnetic resonance spectroscopy at 7 T. Neuroscience 354, 168-177.
Martinez, A., Hillyard, S.A., Dias, E.C., Hagler, D.J., Butler, P.D., Guilfoyle, D.N., Jalbrzikowski, M., Silipo, G., Javitt, D.C., 2008. Magnocellular pathway impairment in schizophrenia: Evidence from functional Magnetic Resonance Imaging. The Journal of Neuroscience 28, 7492-7500.
Mentch, J., Spiegel, A., Ricciardi, C., Robertson, C.E., 2019. GABAergic inhibition gates perceptual awareness during binocular rivalry. The Journal of Neuroscience 39, 8398-8407.
Miller, S.M., Gynther, B.D., Heslop, K.R., Liu, G.B., Mitchell, P.B., Ngo, T.T., Pettigrew, J.D., Geffen, L.B., 2003. Slow binocular rivalry in bipolar disorder. Psychological Medicine 33, 683-692.
Murray, S.O., Kersten, D., Olshausen, B.A., Schrater, P., Woods, D.L., 2002. Shape perception reduces activity in human primary visual cortex. Proceedings of the National Academy of Sciences of the United States of America 99, 15164.
Nagamine, M., Yoshino, A., Miyazaki, M., Takahashi, Y., Nomura, S., 2009. Difference in binocular rivalry rate between patients with bipolar I and bipolar II disorders. Bipolar Disorders 11, 539-546.
Ngo, T.T., Mitchell, P.B., Martin, N.G., Miller, S.M., 2011. Psychiatric and genetic studies of binocular rivalry: An endophenotype for bipolar disorder? Acta Neuropsychiatrica 23, 37-42.
Nurminen, L., Kilpelainen, M., Laurinen, P., Vanni, S., 2009. Area summation in human visual system: Psychophysics, fMRI, and modeling. Journal of Neurophysiology 102, 2900-2909.
Olman, C.A., Ugurbil, K., Schrater, P., Kersten, D., 2004. BOLD fMRI and psychophysical measurements of contrast response to broadband images. Vision Research 44, 669-683.
Olman, C.A., Yacoub, E., 2011. High-field fMRI for human applications: An overview of spatial resolution and signal specificity. The Open Neuroimaging Journal 5, 74-89.
Petrov, Y., McKee, S.P., 2006. The effect of spatial configuration on surround suppression of contrast sensitivity. Journal of Vision 6.
Pihlaja, M., Henriksson, L., James, A.C., Vanni, S., 2008. Quantitative multifocal fMRI shows active suppression in human V1. Human Brain Mapping 29, 1001-1014.
Pokorny, V.J., Espensen-Sturges, T.D., Burton, P.C., Sponheim, S.R., Olman, C.A., 2021a. Aberrant cortical connectivity during ambiguous object recognition is associated with schizophrenia. Biological Psychiatry: Cognitive Neuroscience and Neuroimaging 6, 1193-1201.
Pokorny, V.J., Lano, T.J., Schallmo, M.-P., Olman, C.A., Sponheim, S.R., 2021b. Reduced influence of perceptual context in schizophrenia: behavioral and neurophysiological evidence. Psychological Medicine 51, 786-794.
Poltoratski, S., Ling, S., McCormack, D., Tong, F., 2017. Characterizing the effects of feature salience and top-down attention in the early visual system. Journal of Neurophysiology 118, 564-573.
Provencher, S.W., 2001. Automatic quantitation of localized in vivo 1H spectra with LCModel. NMR in Biomedicine 14, 260-264.
Qiu, C., Burton, P.C., Kersten, D., Olman, C.A., 2016. Responses in early visual areas to contour integration are context dependent. Journal of Vision 16, 19.
Raine, A., 1991. The SPQ: A scale for the assessment of schizotypal personality based on DSM-III-R criteria. Schizophrenia Bulletin 17, 555-564.
Rivolta, D., Castellanos, N.P., Stawowsky, C., Helbling, S., Wibral, M., Grutzner, C., Koethe, D., Birkner, K., Kranaster, L., Enning, F., Singer, W., Leweke, F.M., Uhlhaas, P.J., 2014. Source-Reconstruction of Event-Related Fields Reveals Hyperfunction and Hypofunction of Cortical Circuits in Antipsychotic-Naive, First-Episode Schizophrenia Patients during Mooney Face Processing. Journal of Neuroscience 34, 5909-5917.
Robertson, Caroline E., Ratai, E.-M., Kanwisher, N., 2016. Reduced GABAergic action in the autistic brain. Current Biology 26, 80-85.

Robol, V., Tibber, M.S., Anderson, E.J., Bobin, T., Carlin, P., Shergill, S.S., Dakin, S.C., 2013. Reduced crowding and poor contour detection in schizophrenia are consistent with weak surround inhibition. PLOS ONE 8, e60951.
Saad, Z.S., Glen, D.R., Chen, G., Beauchamp, M.S., Desai, R., Cox, R.W., 2009. A new method for improving functional-to-structural MRI alignment using local Pearson correlation. NeuroImage 44, 839-848.
Schallmo, M.-P., Grant, A.N., Burton, P.C., Olman, C.A., 2016. The effects of orientation and attention during surround suppression of small image features: A 7 Tesla fMRI study. Journal of Vision 16, 19.
Schallmo, M.-P., Murray, S.O., 2016. Identifying seperate components of surround suppression. Journal of Vision 16, 2.
Schallmo, M.-P., Sponheim, S.R., Olman, C.A., 2013. Abnormal contextual modulation of visual contour detection in patients with schizophrenia. PLOS ONE 8, e68090.
Schallmo, M.-P., Sponheim, S.R., Olman, C.A., 2015. Reduced contextual effects on visual contrast perception in schizophrenia and bipolar affective disorder. Psychological Medicine 45, 3527-3537.
Schallmo, M.P., Weldon, K.B., Burton, P.C., Sponheim, S.R., Olman, C.A., 2021. Assessing methods for geometric distortion compensation in 7 T gradient echo functional MRI data. Human Brain Mapping 42, 4205-4223.
Schmack, K., Rothkirch, M., Priller, J., Sterzer, P., 2017. Enhanced predictive signalling in schizophrenia. Human Brain Mapping 38, 1767-1779.
Schmack, K., Schnack, A., Priller, J., Sterzer, P., 2015. Perceptual instability in schizophrenia: Probing predictive coding accounts of delusions with ambiguous stimuli. Schizophrenia Research: Cognition 2, 72-77.
Sclar, G., Maunsell, J.H.R., Lennie, P., 1990. Coding of image contrast in central visual pathways of the macaque monkey. Vision Research 30, 1-10.
Self, M.W., Peters, J.C., Possel, J.K., Reithler, J., Goebel, R., Ris, P., Jeurissen, D., Reddy, L., Claus, S., Baayen, J.C., Roelfsema, P.R., 2016. The effects of context and attention on spiking activity in human visual cortex. PLoS Biology 14, e1002420.
Serrano-Pedraza, I., Romero-Ferreiro, V., Read, J.C.A., Dieguez-Risco, T., Bagney, A., Caballero-Gonzalez, M., Rodriguez-Torresano, J., Rodriguez-Jimenez, R., 2014. Reduced visual surround suppression in schizophrenia shown by measuring contrast detection thresholds. Frontiers in Psychology 5.
Seymour, K., Stein, T., Sanders, L.L.O., Guggenmos, M., Theophil, I., Sterzer, P., 2013. Altered contextual modulation of primary visual cortex responses in schizophrenia. Neuropsychopharmacology 38, 2607-2612.
Shushruth, S., Nurminen, L., Bijanzadeh, M., Ichida, J.M., Vanni, S., Angelucci, A., 2013. Different orientation tuning of near- and far-surround suppression in macaque primary visual cortex mirrors their tuning in human perception. The Journal of Neuroscience 33, 106-119.
Silson, E.H., Reynolds, R.C., Kravitz, D.J., Baker, C.I., 2018. Differential sampling of visual space in ventral and dorsal early visual cortex. The Journal of Neuroscience 38, 2294-2303.
Silverstein, S., Berten, S., Essex, B., Kovacs, I., Susmaras, T., Little, D.M., 2009. An fMRI examination of visual integration in schizophrenia. Journal of Integrative Neuroscience 8, 175-202.
Silverstein, S., Hatashita-Wong, M., Schenkel, L., Wilkniss, S., Kovacs, I., Feher, A., Smith, T., Goicochea, C., Uhlhaas, P., Carpiniello, K., others, 2006. Reduced top-down influences in contour detection in schizophrenia. Cognitive Neuropsychiatry 11, 112-132.
Silverstein, S., Keane, B., Barch, D., Carter, C.S., Gold, J., Kovacs, I., MacDonald, A.W., Ragland, J.D., Strauss, M.E., 2012. Optimization and validation of a visual integration test for schizophrenia research. Schizophrenia Bulletin 38, 125-134.
Silverstein, S.M., Harms, M.P., Carter, C.C., Gold, J.M., Keane, B.P., MacDonald, A., Ragland, J.D., Barch, D.M., 2015. Cortical contributions to impaired contour integration in schizophrenia. Neuropsychologia 75, 469-480.
Silverstein, S.M., Kovacs, I., Corry, R., Valone, C., 2000. Perceptual organization, the disorganization syndrome, and context processing in chronic schizophrenia. Schizophrenia Research 43, 11-20.
Skottun, B.C., Skoyles, J.R., 2007. Contrast sensitivity and magnocellular functioning in schizophrenia. Vision Research 47, 2923-2933.
Slaghuis, W.L., Bishop, A.M., 2001. Luminance flicker sensitivity in positive- and negative-symptom schizophrenia. Experimental Brain Research 138, 88-99.
Snellen, H., 1862. Probebuchstaben zur Bestimmung der Sehschärfe.
Snowden, R.J., Hammett, S.T., 1998. The effects of surround contrast on contrast thresholds, perceived contrast, and contrast discrimination. Vision Research 38, 1935-1945.
Tadin, D., Kim, J., Doop, M.L., Gibson, C., Lappin, J.S., Blake, R., Park, S., 2006. Weakened center-surround interactions in visual motion processing in schizophrenia. The Journal of Neuroscience 24, 11403-11412.
Tibber, M.S., Anderson, E.J., Bobin, T., Antonova, E., Seabright, A., Wright, B., Carlin, P., Shergill, S., Dakin, S.C., 2013. Visual surround suppression in schizophrenia. Frontiers in Psychology 4, 1-13.
Uhlhaas, P.J., Linden, D.E.J., Singer, W., Haenschel, C., Lindner, M., Maurer, K., Rodriguez, E., 2006. Dysfunctional long-range coordination of neural activity during Gestalt perception in schizophrenia. The Journal of Neuroscience 26, 8168.
Van de Moortele, P.F., Akgun, C., Adriany, G., Moeller, S., Ritter, J., Collins, C.M., Smith, M.B., Vaughan, J.T., Uğurbil, K., 2005. B_1 destructive interferences and spatial phase patterns at 7 T with a head transceiver array coil. Magnetic Resonance in Medicine 54, 1503-1518.

Van Essen, D.C., Smith, S.M., Barch, D.M., Behrens, T.E.J., Yacoub, E., Ugurbil, K., 2013. The WU-Minn Human Connectome Project: An overview. NeuroImage 80, 62-79.
van Loon, A.M., Knapen, T., Scholte, H.S., St. John-Saaltink, E., Donner, T.H., Lamme, V.A.F., 2013. GABA shapes the dynamics of bistable perception. Current Biology 23, 823-827.
Vanegas, M.I., Blangero, A., Kelly, S.P., 2015. Electrophysiological indices of surround suppression in humans. Journal of Neurophysiology 113, 1100-1109.
Ventura, J., Nuechterlein, K.H., Subotnik, K.L., Gutkind, D., Gilbert, E.A., 2000. Symptom dimensions in recent-onset schizophrenia and mania: a principal components analysis of the 24-item Brief Psychiatric Rating Scale. Psychiatry Research 97, 129-135.
Vu, A., Jamison, K., Glasser, M.F., Smith, S.M., Coalson, T., Moeller, S., Auerbach, E.J., Uğurbil, K., Yacoub, E., 2017. Tradeoffs in pushing the spatial resolution of fMRI for the 7T Human Connectome Project. NeuroImage 154, 23-32.
Vu, A.T., Auerbach, E., Lenglet, C., Moeller, S., Sotiropoulos, S.N., Jbabdi, S., Andersson, J., Yacoub, E., Ugurbil, K., 2015. High resolution whole brain diffusion imaging at 7 T for the Human Connectome Project. NeuroImage 122, 318-331.
Walker, G.A., Ohzawa, I., Freeman, R.D., 1999. Asymmetric suppression outsize the classical receptive field of the visual cortex. The Journal of Neuroscience 19, 10536-10553.
Wang, L., Mruczek, R.E.B., Arcaro, M.J., Kastner, S., 2015. Probabilistic Maps of Visual Topography in Human Cortex. Cerebral Cortex 25, 3911-3931.
Watson, D., Clark, L., Tellegen, A., 1988. Development and validation of brief measures of positive and negative affect: The PANAS scales. Journal of Personality and Social Psychology 54, 1063-1070.
Webb, B.S., Dhruv, N.T., Solomon, S.G., Tailby, C., Lennie, P., 2005. Early and late mechanisms of surround suppression in striate cortex of macaque. The Journal of Neuroscience 25, 11666-11675.
Wechsler, D., 2008. Wechsler Adult Intelligence Scale, 4th Ed. Pearson Assessment, San Antonio, TX.
Wertheimer, M., 1938. Laws of organization in perceptual forms. In: Ellis, W.D. (Ed.), A source book of Gestalt psychology. Kegan Paul, Trench, Trubner & Company, London, pp. 71-88.
Williams, A.L., Singh, K.D., Smith, A.T., 2003. Surround modulation measured with functional MRI in the human visual cortex. Journal of Neurophysiology 89, 525-533.
Wu, X., Schmitter, S., Auerbach, E.J., Moeller, S., Uğurbil, K., Van de Moortele, P.-F., 2013. Simultaneous multislice multiband parallel radiofrequency excitation with independent slice-specific transmit B1 homogenization. Magnetic Resonance in Medicine 70, 630-638.
Xiao, G., He, K., Chen, X., Wang, L., Bai, X., Gao, L., Zhu, C., Wang, K., 2018. Slow Binocular Rivalry as a Potential Endophenotype of Schizophrenia. Frontiers in Neuroscience 12, 634.
Xing, J., Heeger, D.J., 2000. Center-surround interactions in foveal and peripheral vision. Vision Research 40, 3065-3072.
Xing, J., Heeger, D.J., 2001. Measurement and modeling of center-surround suppression and enhancement. Vision Research 41, 571-583.
Yang, E., Tadin, D., Glasser, D.M., Hong, S.W., Blake, R., Park, S., 2013a. Visual context processing in bipolar disorder: A comparison with schizophrenia. Frontiers in Psychology 4, 1-12.
Yang, E., Tadin, D., Glasser, D.M., Hong, S.W., Blake, R., Park, S., 2013b. Visual context processing in schizophrenia. Clinical Psychological Science 1, 5-15.
Ye, X., Zhu, R.-L., Zhou, X.-Q., He, S., Wang, K., 2019. Slower and less variable binocular rivalry rates in patients with bipolar disorder, ocd, major depression, and schizophrenia. Frontiers in Neuroscience 13, 514.
Yoon, J.H., Maddock, R.J., Rokem, A., Silver, M.A., Minzenberg, M.J., Ragland, J.D., Carter, C.S., 2010. GABA concentration is reduced in visual cortex in schizophrenia and correlates with orientation-specific surround suppression. The Journal of Neuroscience 30, 3777-3781.
Yoon, J.H., Rokem, A.S., Silver, M.A., Minzenberg, M.J., Ursu, S., Ragland, J.D., Carter, C.S., 2009. Diminished orientation-specific surround suppression of visual processing in schizophrenia. Schizophrenia Bulletin 35, 1078-1084.
Yu, C., Klein, S., Levi, D.M., 2001. Surround modulation of perceived contrast and the role of brightness induction. Journal of Vision 1, 18-31.
Yu, C., Klein, S.A., Levi, D.M., 2003. Cross-and iso-oriented surrounds modulate the contrast response function: The effect of surround contrast. Journal of Vision 3, 527-540.
Zenger-Landolt, B., Heeger, D.J., 2003. Response suppression in V1 agrees with psychophysics of surround masking. The Journal of Neuroscience 23, 6884-6893.